STRUCTURAL, OPTICAL AND MULTIFERROIC BEHAVIOR OF TRANSITION METAL BASED DOUBLE PEROVSKITE OXIDES

[1]S.Parthasarathy, [2]S. Mohanty, [3]S. Behera*, [4]S. R. Mishra

[1, 3] Department of Physics, Centurion University of Technology and Management, Bhubaneswar, India.
[2]Department of Physics, Trident Academy of Technology, Bhubaneswar, India.
[4] Department of Chemistry, Gandhi Institute for Education and Technology, Baniatangi, Bhubaneswar Odisha

Abstract

The polycrystalline sample of double perovskite structure Ca_2FeNbO_6 was synthesized by high temperature (1000^0C) solid state reaction route. The room temperature XRD pattern confirmed the formation of new compound with tetragonal crystal structure. The surface morphology (shape, size and distribution of grains and pores) of the pellet sample was recorded using scanning electron microscope (SEM). The optical absorption in the entire visible range with small band gap of these materials aligned them for photovoltaic applications. The existence of both ferroelectric and ferromagnetism properties in the material at room temperature confirms their multiferroic behavior. The optical band gap has been calculated from the spectroscopic analysis, which enables the photo voltaic device application of the material.

Keywords : **Double Perovskite, X-Ray Diffraction, SEM, Multiferroic, Optical properties**

1. Introduction

The magnetic interaction between B and B' ions in double perovskites with general formula $A_2BB'O_6$ leads various magnetic behaviours like multiferroicity, half-metallicity and large magnetoresistance [1-4]. Most of the works on double perovskite oxides with cation on A site as rare-earth or alkaline earth elements and cation at B site as transition metals are explored recently [5-7]. Both the "conduction" and "magnetic" electrons of these materials with similar (d) character interact with each other. The ions of same or different elements take part in the above exchange interactions. In the largest family of DP oxide, special attention is given to Fe-based materials, where B is the paramagnetic Fe^{3+} ion with a local spin S = 5/2 , and B is a fivefold charged non-magnetic cation (e.g., B = Nb^{5+}, Sb^{5+} , Ta^{5+})[8].At the same time maximum no of multiferroic materials suffer from low-temperature transition and small magneto-electric coupling coefficient which limited their applications in industry. Though having quite complex structure than perovskites, double perovskites are still promising for multiferroic for multifunctional devices. Very recently strong multiferroic behavior is reported in few DP oxides like $(BaSr)FeMoO_6$, and $YMn_{0\cdot4}Fe_{0.6-x}Ni_xO_3$ [9-10]. Though a good no of reports are available on the magnetic properties of Fe-based DP, some more works need to be explored. On the other hand, the wide band gap of ferroelectric materials is the prime drawback of them using as photo absorber in solar cells. The reduction of band gap without affecting the ferroelectric nature is necessary for increasing the efficiency of PV cells. Therefore, additional chemical modification of the transition metal in the double perovskite octahedra sites of them is approachable to lower the band band gap without disturbing the ferroelectric behavior. Based on the observed results we have prepared the double perovskite oxide, Mg_2FeNbO_6 and studied the optical and multiferroic properties. It is found that presence of 'Ca' cation leads the strong magnetic interactions and the minimum band gap suggests the usefulness for PV applications.

2. Experimental Procedure

The compound Ca_2FeNbO_4 was prepared by the conventional mixed oxide process using precursors of high purity (≥99.99%) Nb_2O_5, Fe_2O_3, and $CaCO_3$, after obtaining stoichiometric amounts of each material that were then hand-ground in the presence of a dry methanol medium to ensure that they were blended homogenously. The precursors were ground for 2 hours before sieving the fine powder with the aim of achieving an homogenously blended powder. To get the required perovskite phase, the uniformly mixed powder was calcined at 1000°C. Using a hydraulic press and pressure of about 10^5Pa, the calcined powder was formed into cylindrical pellets that were 12 mm in diameter and 2 mm in thickness. A little amount of polyvinyl alcohol (PVA) was added as a binder for electrical measurements. For densification and phase purity, the pellets were sintered at 1050°C. Silver paste was applied to the pellets' two faces as electrodes following sintering, and it was then dried for two hours at 250°C. The pellets were then mounted in a two-terminal sample holder, which was connected internally to an impedance analyzer (Model: PSM-1735, 4NL-LCR, UK), to measure dielectric and impedance properties.Phase purity and structural confirmation were verified via X-ray diffraction (XRD) using a Rigaku ULTIMA diffractometer with CuKα radiation (λ = 1.5406 Å) in the 2θ range of 5°–80° at room temperature. Optical properties and band gap energy, were performed using UV–Visible spectroscopy (Shimadzu-2600, dual-beam spectrophotometer) in the wavelength range of 150–750 nm.Magnetic measurements were performed at room temperature using a vibrating sample magnetometer (VSM), Model: 7410 Series. Ferroelectricity was studied with polarization–electric field (P–E) hysteresis loops and current density–electric field (J–E) measurements using a Radiant Precision LCII Ferroelectric Tester (Model No. P-HVi210KSC), which further confirmed the ferroelectric character of the ceramic.

3. Result and Discussion

3.1. Structural analysis

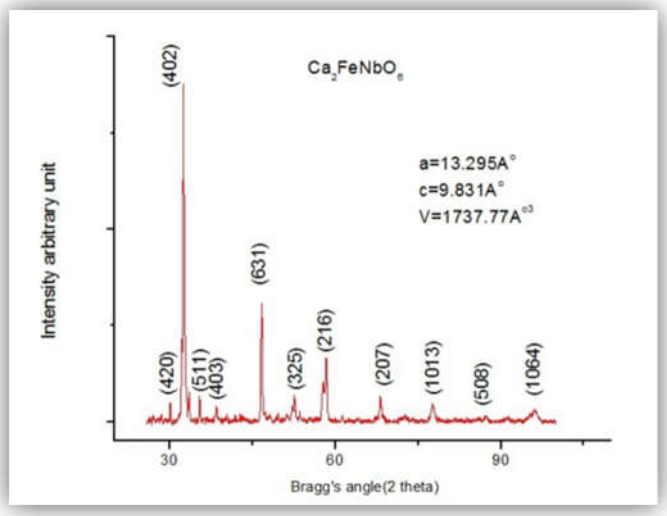

Figure 1. depicts XRD of Ca_2FeNbO_6

The X-ray diffraction pattern (Fig.1) was analyzed using the 'POWD' software to know the crystal structure, lattice parameter and particle size. The appearance of distinct diffraction peaks, to those of the individual precursor oxides, indicates that a new compound was successfully formed in a single-phase perovskite structure. The structural

integrity of the compound was also assessed using the tolerance factor (τ), determined to be 0.979 using for the Goldschmidt tolerance factor formula:

$$\tau = \frac{r_a + r_0}{\sqrt{2}(r_b + r_0)} \quad (1)$$

where r_a and r_b are the average ionic radii of the A-site and B-site cations, respectively, and r_0 is the ionic radius of the oxygen anion. The calculated τ value indicates nearly ideal perovskite structure. The intermediate value of τ between 0.97 and 1 predicts the tetragonal structure of the compound [11].The tetragonal lattice structure was chosen for the compound after fitting the lattice parameter values as : a = 13.295 A^0 , c = 9.831 A^0, c/a=.7267 ,V=1737.77 $(A^0)^3$. Debye-Scherrer relation determines the average particle size value as 36nm [12].

3.2. Microstructural Analysis

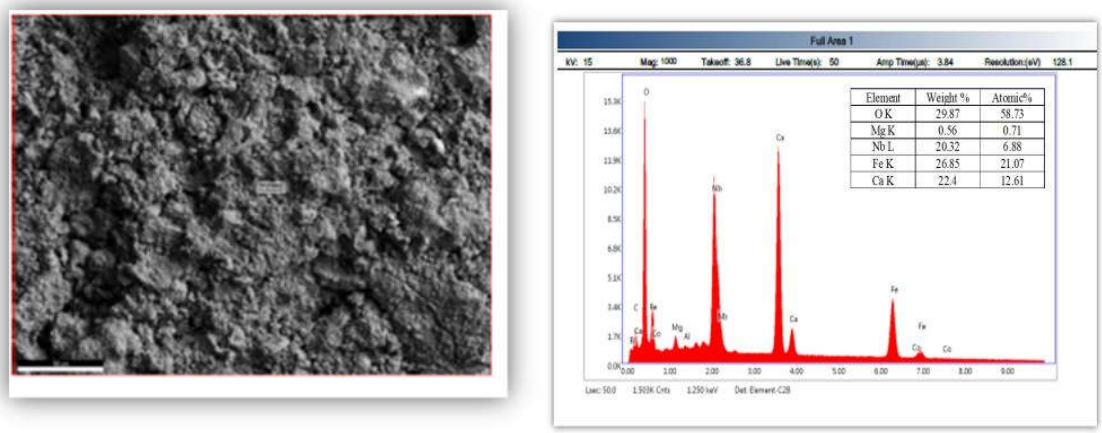

Figure 2. SEM and EDX pattern of Ca_2FeNbO_6

The room temperature surface morphology of the sintered pellet of the ceramic is presented as the SEM image in Fig. 2. The uniform distribution of grains of similar size but different shapes is noticed from the SEM image thus suggesting the polycrystalline nature of the compound. The removal of the binder, carbon dioxide, oxygen vacancies, etc. at high temperature sintering resulted few small voids of irregular dimension in the morphology. The grain size of the compound is found to be in the range of 3–5 μm. The energy dispersive X-ray (EDX) pattern shown in Fig. 2 confirms the components (Ca, Fe, Nb and O) and the composition of the compound. Absence of any foreign elements concludes the purity of the double perovskite material.

3.3. UV-Visible spectroscopy analysis:

The electro-optic nature of the material in the UV to visible range can be analyzed by UV-Visible spectroscopy. The UV–Visible absorption spectrum in Figure 3(a) of the ceramic sample reveals an absorption band from 400–500 nm (visible area), which corresponds to the electronic transitions from half-filled, 2p orbital of O^{2-} ions (valence band), to the vacant 3d orbital of Nb^{5+} ions (conduction band). This transition indicates the absorption edge of Nb [13] confirming it as semiconducting material. Other strong absorption response is observed in the UV area with cutoff wavelength being close to 610 nm, while the visible absorption area ends. The optical band gap (Eg) of the compound was estimated

using the Tauc relation (Mott and Davis model) [14], and the Tauc plot is given in Figure 3(b).

$$(\alpha h\nu)^n = A(h\nu - E_g) \quad (2)$$

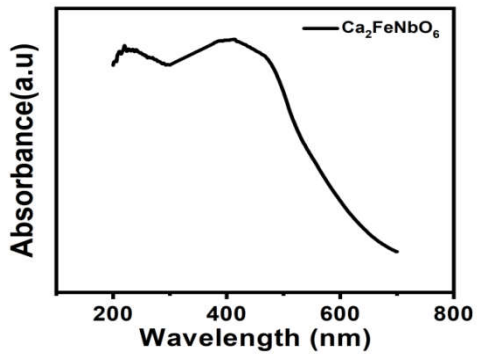

Figure 3(a). Optical absorbance spectrum recorded in the UV–Visible range.

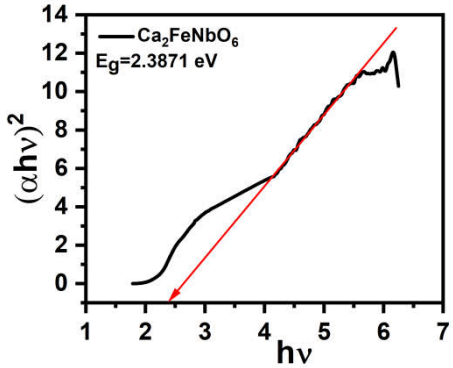

Figure 3(b). shows Tauc plot ($(\alpha h\nu)^2$ vs $h\nu$) graph.

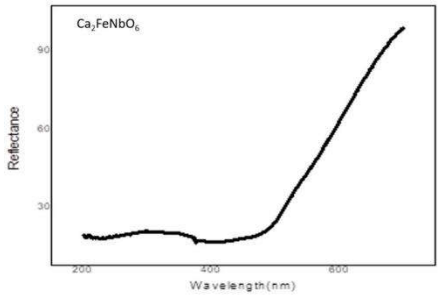

Figure 3(c). UV-Visible reflectance spectra

where α is the absorption coefficient, hν is the photon energy, A is a constant, and n is the transition index that depends on the nature of the electronic transition. According to literature, perovskite-based materials typically exhibit direct allowed transitions, for which the value of n = ½ is considered appropriate. In this study, the band gap was evaluated by extrapolating the linear portion of the $(\alpha h\nu)^2$ vs. hν plot to the energy axis[15]. The reflectance spectra follows reverse trend of absorbance as usually (fig 3(c)). The minimal energy bandgap of present DP oxide comparable with the Silcon based compounds opens up the usefulness for photo voltaic devices and hence in fabrication of solar cells.

3.4. Ferroelectric study

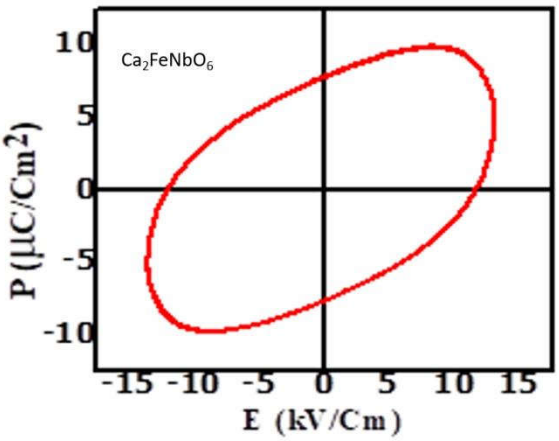

Figure 4. depicts the Ferroelectric hysteresis loop

The induced polarization is varied with the applied electric field to know about the ferroelectric behavior of the oxide material and is shown in fig 4. The presence of a significant remnant polarization in the compound ensures the existence of ferroelectricity in the compound. The loops with rounded corners in the (P-E) hysteresis loop indicated the existence of leakage currents in the bulk ceramic oxide. This leakage is mainly due to Fe and Ca possibly volatizing, from their cationic sites, at high temperature. Furthermore, the large cell area of the loops suggests that the material is lossy because of conduction losses and dielectric relaxation effects.

3.5. Leakage current density with electric field

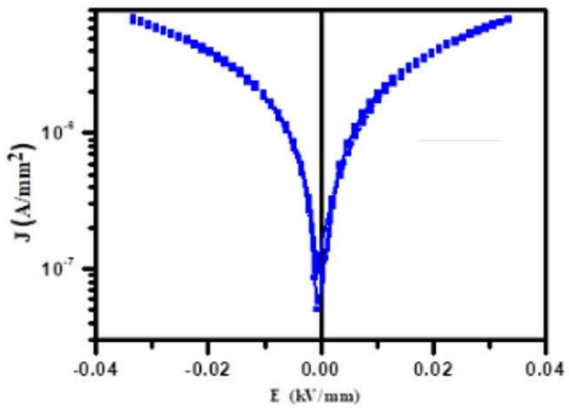

Figure 5. Leakage current vs electric field

The information of current density (J) vs applied electric field (E) at room temperature, recorded at both positive and negative bias, is shown in Fig. 5, showing the insulating behavior of the material. From here we considered the energy storage properties based on

the leak current density change with the applied sinusoidal electric field. We found that at both polarities of the electric field, the leak current density was below 10^{-5}A/cm², suggesting reasonably good insulation properties. This leakage current is likely due to oxygen vacancies in which Fe^{2+} and Fe^{3+} can coexist as different valence states and therefore can create free charge carriers that can be excited under an external electric field [16].

3.6. Magnetization Study

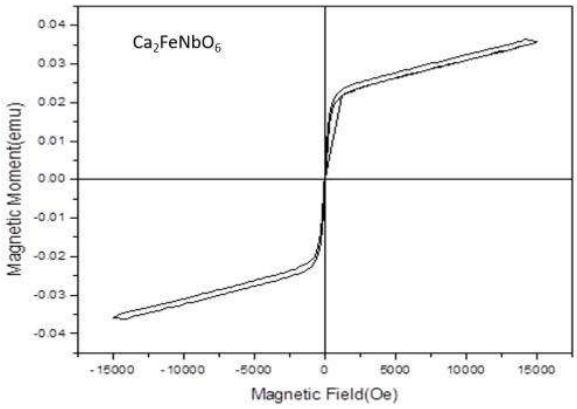

Figure 6. represents the M~H curve

Figure 6 presents the magnetization versus magnetic field (M-H) loop of the synthesized compound measured in room temperature with an applied magnetic field of ±15 kOe. The loop was characterized by low coercivity, negligible remnant magnetization, and low hysteresis indicative of soft ferromagnetism. The magnetic response observed is induced by valence fluctuations among the B-site cations (particularly Fe^{3+}/Fe^{2+} or Nb^{5+}), thereby allowing ferromagnetic interactions across long range superexchange pathways (e.g., Fe^{3+}(or Fe^{2+})-O-Nb^{5+}-O-Fe^{3+}(or Fe^{2+})). These long phase interactions permit weak cooperative spin alignments, yielding the observed soft ferromagnetic nature of the double perovskite oxide [17].

4. Conclusions

The high-temperature mixed oxide route is adopted to prepare the material Ca_2FeNbO_6. The tetragonal structure of the compound is confirmed from the preliminary XRD pattern. The polycrystalline nature of the material with uniform distribution of grain with distinct grain boundaries are is known from the morphological study. The sample's relatively low optical band gap energy of approximately 2.38 eV indicates it could be useful for photovoltaic devices in the region of visible light. The P~E loop and M~H loop studies have provided that the double perovskite material is multiferroic in nature which is useful for the possible device applications.

References:

1) S. Ravi, "Multiferroism in Pr_2FeCrO_6 perovskite," Journal of Rare Earths, (2018), doi: 10.1016/j.jre.2018.03.023.
2) R. Das and R. N. P. Choudhary, "Studies of electrical, magnetic and leakage-current characteristics of double perovskite: Dy_2CoMnO_6," Journal of Alloys and Compounds, vol. 853, (2021), 157240.
3) K. I. Kobayashi, T. Kimura, Y. Tomioka, H. Sawada, and K. Terakura, "Intergrain tunneling magnetoresistance in polycrystals of the ordered double perovskite Sr_2FeReO_6," Physical Review B: Condensed Matter, vol. 59, (1999), 11159.
4) H. Kawanaka, I. Hase, S. Toyama, and Y. Nishihara, "Electronic state of Fe in double perovskite oxide Sr_2FeWO_6," Journal of the Physical Society of Japan, vol. 68, (1999), 2890.
5) S. Bhattacharjee, Materials Science in Semiconductor Processing, (2020), https://doi.org/10.1016/j.mssp.2020.105503.
6) R. Sridharan, Ceramics International, (2017), http://dx.doi.org/10.1016/j.ceramint.2017.07.217.
7) M. Alam and K. Mandal, "Room temperature ferromagnetism and ferroelectricity in double perovskite Y_2NiMnO_6 thin film," Journal of Magnetism and Magnetic Materials, vol. 512, (2020), 167062.
8) N. Benkhaleda, M. Djermounia, A. Zaouia, I. Kondakova, C. Kuzianc, R. Hayne, and H. R. Hayne, "Magnetic properties of the multiferroic double perovskite lead iron niobate: Role of disorder," Journal of Magnetism and Magnetic Materials, vol. 515, (2020), 167309.
9) R. Das and R. N. P. Choudhary, "Structural and electrical properties of double perovskite: (BaSr)$FeMoO_6$," Physica B: Physics of Condensed Matter, (2020), doi: https://doi.org/10.1016/j.physb.2020.412522.
10) S. Chihaoui, N. Kharrat, M. A. Wederni, M. Koubaa, W. CheikhrouhouKoubaa, L. Sicard, A. Cheikhrouhou, and K. Khirouni, "Impact of Ni doping on the morphological, electrical and dielectric properties of $YMn_{0\cdot4}Fe_{0\cdot6-x}Ni_xO_3$ ($0 \leq x \leq 0.1$) multiferroics," Physica B: Physics of Condensed Matter, (2021), doi: https://doi.org/10.1016/j.physb.2020.412748.
11) R. Das and R. N. P. Choudhary, Journal of Materials Science: Materials in Electronics, https://doi.org/10.1007/s10854-018-0036-7.
12) E. Wu, "POWD, an interactive program for powder diffraction data interpretation and indexing," Applied Crystallography, vol. 22, no. 5, (1989), pp. 506–510..
13) B. N. Parida, P. Biswal, and R. Padhee, Journal of Materials Science: Materials in Electronics, vol. 31, (2020), pp. 6097–6108.
14) F. P. Keburis, J. Banys, A. Brilingas, J. Prapuolenis, A. Kholkin, and M. E. V. Costa, Ferroelectrics, vol. 353, (2007), p. 149.
15) M. N. Palamaru, V. Musteata, N. Lupu, and L. Mitoseriu, Journal of Alloys and Compounds, doi.org/10.1016/j.jallcom.2015.07.13.
16) A. Anwar, M. A. Basith, and S. Choudhury, "From bulk to nano: A comparative investigation of structural, ferroelectric and magnetic properties of Sm and Ti co-doped $BiFeO_3$ multiferroics," Materials Research Bulletin, (2018), https://doi.org/10.1016/j.materresbull.2018.11.003.
17) Y. Lu, Z. Pai, H. Wu, W. Xia, and X. Zhu, Journal of Materials Science: Ceramics, (2020), https://doi.org/10.1007/s10853-019-04329-3.